

Chapter 2

Background and Theoretical Framework

2.1 Graphene Basics

A flat one atom thick layer of carbon atoms arranged in a honeycomb lattice is known as graphene. The study of graphene dates back to 1947 when Wallace [1] applied band theory to the study of one-atom thick layer of graphite as a building block for the three dimensional material [1, 2]. In 1984, graphene was predicted to be an excellent condensed matter analogue of $(2 + 1)$ -dimensional quantum electrodynamics [3], however this remained just as an ‘academic’ prediction. The great interest in carbon-based materials reached a peak in the 1990s with the discovery of carbon nanotubes [4]. The properties of these virtually one-dimensional materials are easily understood through the ones of two-dimensional graphite [5]. The International Union of Pure and Applied Chemistry (IUPAC) gave the following definition of graphene in 1994 “the term graphene should be used to designate the individual carbon layers in graphite intercalation compounds” [6]. In spite of the theoretical importance of graphene, it was regarded as a virtual material since it was believed to be unstable with respect to the formation of curved structures such as fullerenes and carbon nanotubes. Few-layer graphite on a substrate was an experimental reality much before 2004, but it is not until that year when the Manchester group lead by Novoselov and Geim discovered free-standing graphene [7]. The two-dimensional nature of graphene was quickly confirmed [8] and, more importantly, the behavior of its carriers as massless Dirac fermions [9]. A new definition was given by Geim in a recent review: “graphene is a single atomic plane of graphite which—and this is essential—is sufficiently isolated from its environment to be considered free-standing” [10]. Since 2005, close to ten thousand articles have been published with the word ‘graphene’ on their title¹ and graphene is known for some record-breaking material properties. In addition to being the thinnest and strongest known material in the universe, “its charge carriers exhibit giant intrinsic mobility, have zero effective mass, and can travel for micrometers without scattering at room temperature.

¹ Data taken from ISIWEB up to 2011.

Graphene can sustain current densities six orders of magnitude higher than that of copper, shows record thermal conductivity and stiffness, is impermeable to gases, and reconciles such conflicting qualities as brittleness and ductility” [10]. In recognition for their pioneering work, Geim and Novoselov won the Nobel Prize in Physics in 2010 “for groundbreaking experiments regarding the two-dimensional material graphene”.

Apart from its outstanding mechanical and optical properties, the most relevant feature of graphene related to transport is its low-energy dispersion relation. The Fermi surface of graphene at half-filling is reduced to six points where two equivalent bands touch. Due to the honeycomb lattice symmetry of graphene only, two of these points are relevant. In the low-energy regime, the two equivalent bands of graphene reduce to two conical bands (referred to as “valleys”) that touch at the two inequivalent charge neutrality points known as “Dirac points”. The behavior of charge carriers in this regime is analogous to that of massless Dirac fermions. As a consequence, graphene offers the possibility to experimentally probe interesting phenomena that is usually out of experimental range. This striking property triggered a wave of research activity in the condensed matter community. A wide range of high-energy phenomena, such as half-integer quantum Hall effect and Klein tunneling, were predicted and measured in graphene.

Graphene exhibits another fascinating property. In spite of having relatively weak electronic correlations, varied phenomena such as ferromagnetism and superconductivity can be induced in graphene by proximity to a host material. Indeed, depositing a graphene layer on top of a superconducting electrode, the region of the layer that covers the superconductor inherits the pairing correlation between electrons and holes by means of the proximity effect [11–14]. This peculiarity opened a wide range of possibilities. In particular, it allowed the study of the rich interplay between superconductivity and relativistic phenomena in graphene-superconductor hybrid structures.

Due to the “short life” of graphene and the immense interest on it, any attempt to produce an up-to-date review of its properties quickly became obsolete. The basic properties of graphene have been known for sixty years and, although it is easy to find detailed reports on the basic transport properties of graphene, new review articles appear frequently to account for the most recent experimental and theoretical updates. A list of the most recent and complete reviews is provided as follows. A good review of the new interesting transport properties of graphene can be found in Ref. [15], although the basics about the low-energy dispersion relation of graphene were clearly exposed in the articles by Wallace [1], Slonczewski and Weiss [2] and Semenoff [3]. Similarly, Ref. [5] reviews the case of carbon nanotubes, which is frequently analogous to that of graphene. A more thorough and updated review for the transport properties of graphene is found in Ref. [16]. The similarities between the tight-binding approach and the continuous quantum electrodynamics model in two-dimensions, with special emphasis on the symmetries, are described in Ref. [17]. Reference [18] gives a short introduction to the interplay between relativistic Dirac particles and superconductivity. Klein tunneling and negative refraction are reviewed in a very pedagogical way in Ref. [19]. An updated overview of the fabrication and

electronic properties of graphene nanostructures, with a detailed description of recent reports on graphene-based quantum dots can be found in Ref. [20]. In the same line, Ref. [21] provides both experimental and theoretical updates and Ref. [22] argues for the application of graphene-based quantum dots for spin *qubits* from a theoretical point of view. Finally, the effect of disorder on the transport properties of graphene has been recently reviewed in Ref. [23] and briefly in Ref. [24].

This chapter is organized as follows: We begin by introducing a microscopic tight-binding model for graphene which accounts for many of its basic characteristics. Specifically, we explain how the low energy excitations of graphene within the tight-binding approximation can be effectively described using the Dirac equation. We proceed to explore the relativistic behavior of charge carriers in graphene, emphasizing striking properties like Klein tunneling, pseudo-diffusive transport, the minimum of conductivity and the appearance of charge puddles. Next, we introduce the superconducting proximity effect in metal-superconductor hybrid structures. We explain how the Andreev reflection mechanism is the microscopic process that can be used to describe transport in such systems. We consider the special Andreev reflection in graphene, highlighting its differences with the case of normal metals. Finally, we briefly introduce the basics of the nonlocal transport in a three terminal device.

2.1.1 From the Tight-Binding Model to the Dirac Equation

In this section, we derive the band structure of graphene within the tight-binding approximation. From the energy dispersion relation of graphene we obtain the Dirac equation in the low-energy regime. This derivation was first introduced by Wallace in 1947 [1] when studying the band theory of graphite. The results presented here are analogous to that work.

The honeycomb structure of graphene is formed by combining two triangular lattices, denoted A and B, or equivalently, a triangular lattice with a basis of two atoms per unit cell. A unit cell contains one atom from each lattice and thus the vectors $\mathbf{a}_{1,2} = (1, \pm\sqrt{3})a/2$ are defined as the primitive translations and $a = |\mathbf{a}_1| = |\mathbf{a}_2| = \sqrt{3}a_0 \approx 0.246 \text{ nm}$ is the lattice constant. A schematic of the graphene lattice is shown in Fig. 2.1a. The corresponding reciprocal lattice vectors are $\mathbf{b}_{1,2} = (1, \pm 1/\sqrt{3})2\pi/a$.

Any atom from a determined sublattice, say A, is connected to its three nearest neighbors from the other sublattice, B, via the vectors $\delta_1 = (\mathbf{a}_1 - \mathbf{a}_2)/3 = (0, 1/\sqrt{3})a$, $\delta_2 = \mathbf{a}_1/3 + 2\mathbf{a}_2/3 = (1, -1/\sqrt{3})a/2$ and $\delta_3 = -2\mathbf{a}_1/3 - \mathbf{a}_2/3 = (1, -1/\sqrt{3})a/2$ (see Fig. 2.1a). Consequently, any pair of atoms from a unit cell can be labeled through the integers n_1 and n_2 by the vectors $\mathbf{R}_A = n_1\mathbf{a}_1 + n_2\mathbf{a}_2$ and $\mathbf{R}_B = n_1\mathbf{a}_1 + n_2\mathbf{a}_2 + \delta_1$.

The carbon atoms in the graphene plane are connected by strong covalent bonds due to the sp^2 hybridization of the atomic orbitals $2s$, $2p_x$ and $2p_y$. The $2p_z$ orbitals are perpendicular to the graphene plane, have zero overlap with the rest and can be treated independently. They form the π bonds of graphene, while the in-plane overlap

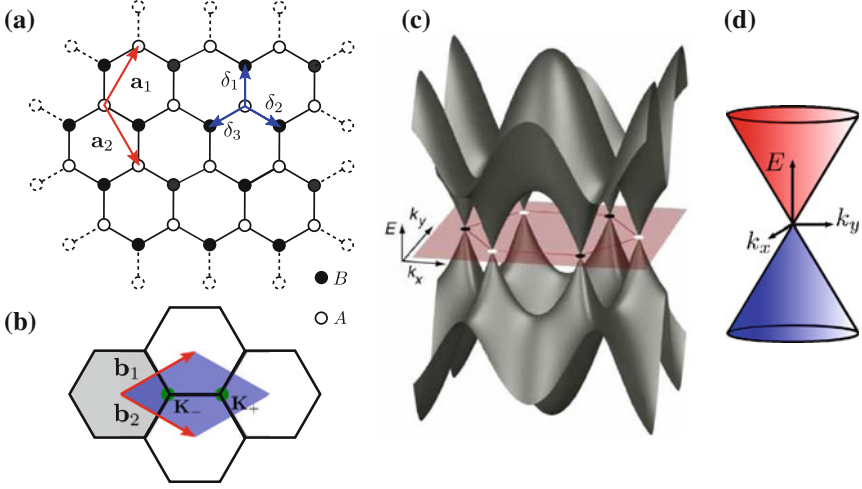


Fig. 2.1 **a** Graphene lattice showing the sublattices A and B and the primitive translations. **b** Brillouin Zone of graphene showing the reciprocal lattice vectors and the Dirac points \mathbf{K}_+ and \mathbf{K}_- . **c** Graphene dispersion relation evaluated from Eq.(2.2). Reprinted figure with permission from Beenakker [18]. Copyright (2008) by the American Physical Society. **d** Low energy dispersion relation around any of the Dirac points from Eq.(2.5), showing in *blue* the valence band and in *red* the conduction band

is called a σ bond. We can thus provide a basis of wavefunctions for the lowest energy states in graphene using two Bloch functions constructed from the atomic orbitals for the two inequivalent carbon atoms at A and B sites,

$$\Phi_i(\mathbf{r}) = \frac{1}{\sqrt{N}} \sum_{\mathbf{R}_i} e^{i\mathbf{k}\mathbf{R}_i} \varphi(\mathbf{r} - \mathbf{R}_i), \text{ with } i = A, B.$$

N is the number of unit cells, $\varphi(\mathbf{r})$ is the normalized $2p_z$ orbital of the isolated carbon atom and the summation is taken over all possible lattice vectors. From the Schrödinger equation $\mathbf{H}\Psi = E\Psi$, with $\Psi = C_A\Phi_A + C_B\Phi_B$, one can obtain the transfer integral matrix $H_{ij} = \langle \Phi_i | H | \Phi_j \rangle$ and the overlap integral matrix $S_{ij} = \langle \Phi_i | \Phi_j \rangle$. The energy dispersion relation for the system is obtained from the secular equation $\det[\mathbf{H} - E\mathbf{S}] = 0$. Since the two atoms of the unit cell are identical, the Hamiltonian matrix element H_{AA} , which represents the interaction of an atom at site A with itself and the rest of the A atoms in the lattice, is exactly the same as H_{BB} . It follows that $H_{AB} = H_{BA}^*$. One can further neglect the overlap between wave functions centered at different atoms which makes $S_{AB} = S_{BA} = 0$. Lastly, assuming a proper normalization of the wave functions leads to $S_{AA} = S_{BB} = N$. Under these approximations the secular equation is reduced to $E^\pm = H_{AA} \pm |H_{AB}|$, where E^\pm represents the eigenvalue for the symmetric combination of wave functions that

form the valence band or the bonding π energy band, and E^- is the antisymmetric conduction band or the anti-bonding π^* band.

Within the nearest neighbors tight-binding approximation, every atom, A , interacts only with itself and the surrounding three B atoms and vice versa. The diagonal elements thus become constant terms representing the energy of an electron on the $2p_z$ orbital of carbon, including the effect of the periodic potential of the lattice: $H_{AA} = E_{2p}$. If the atoms of the unit cell were inequivalent, as it is the case for boron nitride (BN), the on-site energy E_{2p} would be different for B and N and the dispersion relation would show a gap between the π and π^* bands. That is not the case of graphene (which formed only by carbon atoms) and we can thus state that $E_{2p} = E_F = 0$.

The off-diagonal terms are

$$\begin{aligned}
 H_{AB} &= H_{BA}^* = \langle \Phi_A | H | \Phi_B \rangle \\
 &= \sum_{\mathbf{R}_A} \sum_{\mathbf{R}_B} e^{i\mathbf{k}(\mathbf{R}_A - \mathbf{R}_B)} \langle \varphi(\mathbf{r} - \mathbf{R}_A) | H | \varphi(\mathbf{r} - \mathbf{R}_B) \rangle \\
 &= t_g \sum_{\delta_i} e^{i\mathbf{k}\delta_i} = t_g e^{i\mathbf{k}(\mathbf{a}_1 - \mathbf{a}_2)/3} \left[1 + e^{i\mathbf{k}\mathbf{a}_2} + e^{-i\mathbf{k}\mathbf{a}_1} \right] \\
 &= t_g \left[\exp\left(i \frac{k_y a}{\sqrt{3}}\right) + 2 \cos \frac{k_x a}{2} \exp\left(-i \frac{k_y a}{2\sqrt{3}}\right) \right], \tag{2.1}
 \end{aligned}$$

where we have used the radial symmetry of wave functions φ_i in the graphene plane and the single value of the nearest neighbor distance to define the tight-binding integral $t_g > 0$. The substitution into the secular equation is straightforward and the resulting energy dispersion relation for a graphene plane in the tight-binding approximation is

$$E^\pm(k_x, k_y) = E_F \pm t_g \sqrt{1 + 4 \cos^2 \frac{k_x a}{2} + 4 \cos \frac{k_x a}{2} \cos \frac{\sqrt{3} k_y a}{2}}. \tag{2.2}$$

Since graphene's honeycomb lattice contains two atoms per unit cell (two sublattices) the excitation spectrum contains two branches (bands) which are symmetrical around $E = 0$ (see Fig. 2.1c). These bands touch at six points in momentum space given by the roots of $E(\mathbf{k}) = 0$

$$\begin{aligned}
 k_x &= \pm \frac{4\pi}{3a}, \quad k_y = 0 \\
 k_x &= \pm \frac{2\pi}{3a}, \quad k_y = \pm \frac{2\pi}{\sqrt{3}a}. \tag{2.3}
 \end{aligned}$$

At half-filling of the bands, which is the pertinent situation for the study of graphene and other carbon-based materials, the band structure given by Eq. (2.2) has six isolated Fermi points instead of a Fermi line. These are the six corners of the

first Brillouin zone which, due to the symmetry of the hexagonal lattice, correspond to only two independent states. This result is of capital importance in research since it allows to study the low-energy excitations of graphene by taking the continuum limit at any two independent Fermi points. For example, if we choose the two independent Fermi points

$$\mathbf{K}_{\pm} = (\pm \frac{4\pi}{3a}, 0), \quad (2.4)$$

any wave vector in the proximity of \mathbf{K}_{\pm} can be written as $\mathbf{k} = (\pm \frac{4\pi}{3a} + \delta k_x, \delta k_y)$. By substituting in Eq. (2.1) we obtain

$$\begin{aligned} t_g \left[\exp \left(i \frac{\delta k_y a}{\sqrt{3}} \right) + 2 \cos \left(\pm \frac{2\pi}{3} + \frac{\delta k_x a}{2} \right) \exp \left(-i \frac{\delta k_y a}{2\sqrt{3}} \right) \right] \\ \approx \pm \frac{\sqrt{3}}{2} t_g a (\delta k_x \mp i \delta k_y) + \mathcal{O} \left((a \delta \mathbf{k})^2 \right). \end{aligned}$$

It follows that, consequently,

$$E^{\pm}(\mathbf{k}) \approx \pm \frac{\sqrt{3}}{2} t_g a |\mathbf{k}| = \pm \hbar v_F |\mathbf{k}|. \quad (2.5)$$

This result implies that the energy dispersion relation is conical in the proximity of a Fermi point. A striking consequence is that the Fermi velocity, defined as $\hbar v_F = \sqrt{3} t_g a / 2$, is independent of both the electronic energy and momentum. The best experimental estimates of $t_g \approx 2.5$ eV and $a \approx 0.14$ nm result in a $v_F \approx 10^6$ m/s in the absence of any carriers. In the presence of charge carriers this value is slightly modified without affecting the results presented here [16]. The linearity of the dispersion relation continues up to an energy $E_C < 0.4 t_g \sim 1$ eV, which allows to introduce a cutoff wave vector $k_c = E_C / \hbar v_F \approx 0.25$ nm⁻¹.

In the usual continuum approximation for lattice theories in condensed matter physics, i.e. the effective mass theory, one has a quadratic dispersion relation. An effective Schrödinger equation can be implemented in which all many-body effects are included in the effective mass parameter. In contrast, graphene is a zero band-gap semiconductor with a linear low-energy dispersion for electrons and holes in the conduction and valence bands, respectively.

The linearity of the dispersion relation, with an energy independent Fermi velocity, is not the only outstanding result for the low-energy spectra of graphene. Having two atoms per unit cell or two equivalent and independent sublattices A and B implies that the two linear branches of the dispersion relation become independent of each other. This degree of freedom due to the sublattices defines a *pseudospin* quantum number equivalent to the electron spin. The resulting low-energy, long-wavelength, effective 2D continuum Schrödinger equation for spinless carriers in the proximity of graphene Fermi point \mathbf{K}_{\pm} becomes

$$- \hbar v_F \begin{pmatrix} 0 & \pm k_x - i k_y \\ \pm k_x + i k_y & 0 \end{pmatrix} \begin{pmatrix} \Phi_A^\pm(\mathbf{k}) \\ \Phi_B^\pm(\mathbf{k}) \end{pmatrix} = (E - E_F) \begin{pmatrix} \Phi_A^\pm(\mathbf{k}) \\ \Phi_B^\pm(\mathbf{k}) \end{pmatrix}. \quad (2.6)$$

$\Phi^\pm(\mathbf{k}) = (\Phi_A^\pm(\mathbf{k}), \Phi_B^\pm(\mathbf{k}))^T$ is a 2D spinor wave function for the pseudospin degree of freedom. Equation (2.6) is exactly the equation for massless chiral Dirac fermions in 2D, known as Weyl's equation for neutrinos, with the only difference that the spinor acts on the pseudospin space rather than on the real spin. We refer to the Fermi points of Eqs. (2.3) and (2.4) as *Dirac* points or *valleys*. A complete low-energy description of charge carriers in graphene is realized by combining the Dirac equation for each valley in a 4×4 structure. When intervalley scattering can be neglected, the results for each valley are equivalent and one can ignore the valley degree of freedom. Intervalley scattering requires a large momentum transfer or strong lattice scale scattering. It is therefore weak and usually ignored in the description of the low energy states in graphene.

A series of experiments conducted by the Manchester group lead by Geim triggered an intense research activity on graphene. Not only did they isolate graphene but also demonstrated the relativistic behavior of electrons. In Ref. [7], the method to obtain one-atom thick graphite was presented. It was further developed in Ref. [8]. It was demonstrated that few and also mono layer graphite behaved like a two dimensional semimetal. There was a small overlap between the conduction and the valence bands and a strong ambipolar electric field effect was measured. In Ref. [9] the relativistic behavior of carriers in graphene was demonstrated. A linear dependence of the conductivity on the gate voltage was measured. Mobilities up to $15,000 \text{ cm}^2 \text{ V}^{-1} \text{ s}^{-1}$ were measured for electrons and holes. Lastly, the measurement of half-integer quantum Hall effect corroborated once more the two-dimensional relativistic nature of carriers in graphene.

2.1.2 Relativistic Behavior of Low-Energy Carriers in Graphene

Wave functions around each Dirac point satisfy Eq. (2.6), with E being the excitation energy of an electron-like quasiparticle. If we assume that momentum along the y -axis ($\hbar q$) is conserved, the wave function can be written as $\Phi_\pm(x, y) = e^{iqy} \phi_\pm(x)$. With the replacement $\mathbf{k}(q) = (-i\partial_x, q)$ in Dirac's equation, we obtain the following linear independent solutions for each valley

$$\begin{aligned} \phi_+(x) &= c_1^+ e^{ikx} \varphi_1 + c_2^+ e^{-ikx} \varphi_2 \\ \phi_-(x) &= c_2^- e^{ikx} \varphi_2 + c_1^- e^{-ikx} \varphi_1, \end{aligned}$$

with

$$\varphi_{1,2} = \begin{pmatrix} 1 \\ \pm s e^{\pm i\alpha} \end{pmatrix}, \quad (2.7)$$

$s = \text{sgn}(E + E_F)$ and $e^{\pm i\alpha} = \hbar v_F(k \pm iq)/(E_F + E)$. The constants $c_{1,2}^{\pm}$ are determined by boundary conditions for the wave functions $\phi_{\pm}(x)$. In a one-valley description of graphene Eq. (2.7) describes an oscillating wave where s is the band index ($s = 1$ for the conduction band and $s = -1$ for the valence band) and $\alpha(\mathbf{k})$ is the angle between the wave vector \mathbf{k} and the x -direction. Let us define the chirality operator as the projection of the pseudo-spin operator on the momentum direction.²

$$\hat{C} \equiv \frac{\mathbf{k} \cdot \hat{\mathbf{e}}}{|\mathbf{k}|}.$$

In the absence of an external potential, this operator commutes with the Hamiltonian and becomes a conserved quantity. The eigenvalues of the chirality are given by the band index $s = \pm 1$. The velocity operator can be defined as $\hat{\mathbf{v}} \equiv -i[\mathbf{r}, \hat{H}] = \hat{\mathbf{e}}$. The average velocity of a plane wave is given by $\mathbf{v} = s\mathbf{k}/|\mathbf{k}|$. As a result, an electron and a hole propagating in the valence band have the same average velocity and move in the same direction. Their electric current is opposite since they have opposite charge.

An important consequence of the conservation of chirality is the absence of backscattering. Any two electron states propagating in opposite directions have opposite chirality, resulting in vanishing probability for reflection. This fact was first exposed by Ando for the one-dimensional case of carbon nanotubes [25, 26].

Another notable property of graphene is the relativistic transmission through a potential barrier, also known as Klein tunneling [27]. A classical barrier confines all particles with energy lower than the barrier height. In quantum mechanics, the wave function of non-relativistic particles with energy lower than the barrier height can still leak out into the classically forbidden region, giving rise to quantum tunneling. It is well known that the transmission through such quantum barrier decreases exponentially with the height and width of the barrier. On the other hand, the transmission probability for Dirac particles depends only weakly on the barrier height, approaching unity with increasing barrier height [28]. As demonstrated in the previous sections, the Dirac Hamiltonian allows for both positive and negative energy states, i.e. electrons and holes. While a potential barrier is repulsive for electrons, it is attractive for holes. The opposite happens for a potential well. At any potential barrier one needs to match the electronic states outside the barrier with the hole states inside. The larger the barrier is, the more complete the matching between electron and hole states is and thus the transmission is greater. As a consequence, the transmission becomes perfect for an infinite barrier.

Effectively, Klein tunneling is a relativistic effect in which electrons and holes are coupled by means of an electrostatic potential. The conservation of chirality that prevents backscattering in graphene is another consequence of the analogy of charge carriers in graphene with relativistic massless Dirac fermions. Tunneling

² This is in fact the helicity operator, which is a function of physical quantities and thus has physical sense. However, in the relativistic limit with zero effective mass both quantities are the same. We adopt the standard in the literature and hereon we call this quantity chirality instead of helicity.

through a potential barrier happens with unit efficiency at normal incidence [28]. An important conclusion is that graphene pn junctions are essentially transparent. This fact has been demonstrated experimentally in several works [29–33]. It is also the reason why graphene-based quantum dots are so experimentally challenging [20–22]. Away from normal incidence, graphene pn junctions behave as negative refraction index interfaces [34]. An unusual possibility for the confinement of massless Dirac fermions involving the use of inhomogeneous magnetic fields [35] has triggered an intense research activity.

A direct consequence of Klein tunneling in graphene is that both the pn junction and the $n'-n-n'$ junctions have finite transmission coefficients. More importantly, graphene's conductivity at zero doping, i.e. at the Dirac point, is finite [36, 37]. A graphene sheet contacted by two heavily electron doped contacts allows the testing of ballistic conductivity at the Dirac point. By *ballistic* conductivity we are referring to the case of noninteracting electrons at zero temperature in the limit of no disorder. The absence of scattering in a non-Dirac metal means that the semiclassical electrical conductivity is infinite, since there is nothing to impede electron motion. The same argument implies that the conductivity would vanish as carrier density is tuned to zero, giving rise to a metal-insulator transition.

The conductivity of a system governed only by the Dirac equation (2.6) can be obtained by calculating the transmission probability of modes confined in a strip of width W and length L that is connected to heavily doped contacts [36, 37]. For transport along the \hat{x} -direction, the transmission probability for a transverse mode has the form

$$T_n = \frac{1}{\cosh^2(q_n L)}, \quad (2.8)$$

where the transverse momentum q_n depends on the detailed boundary condition of the strip [37, 38]. This transmission probability is given strictly by evanescent modes since both the energy and the doping are zero at the Dirac point. It is important to stress that this result is obtained in the absence of disorder, interactions and at zero temperature, i.e. this is a ballistic transmission with a dependence on the length of the sample L . Such dependence, along with the distribution of eigenvalues of the transmission matrix, resembles that of a diffusive system. This property is known as *pseudo-diffusivity* of graphene at the charge neutrality point [39, 40]. More details on the distribution of eigenvalues of the transmission matrix are given in Appendix B.

For wide enough strips, the conductivity of the system is independent of the boundary conditions and is found by summing over the modes,

$$\begin{aligned} \sigma &= g_s g_v \frac{L}{W} \frac{e^2}{h} \sum_n T_n(\hat{x}) = \frac{e^2}{h} \frac{2L}{\pi} \int_{-\infty}^{\infty} \frac{dq}{\cosh^2(qL)} \\ &= \frac{4}{\pi} \frac{e^2}{h} \quad \text{for } W \gg L. \end{aligned} \quad (2.9)$$

The condition for the existence of a well defined (size independent) conductivity is the dependence of the transmission probability on the product qL (Eq. 2.8) and the linear dispersion of the carriers. The condition $W \gg L$ allows the sum of the transmissions over the modes to be written as an integral over q in Eq. (2.9). The key features for a minimum of conductivity are the gapless character of the spectrum and the chirality of the carriers.

In the previous framework, the chemical potential was assumed to be constant throughout the graphene layer, with a discontinuity at the electrodes. This simplification was proven to be insufficient. It is now well known that the spatial distribution of charge close to the Dirac point is not uniform. In low doped graphene, as in other 2D semiconductors, strong charge inhomogeneities appear. These inhomogeneities are known as electron-hole puddles³ and are due to a random distribution of charge in the environment and, in a small part, to the ripples associated with the substrate roughness or the intrinsic wrinkles of suspended graphene. Contrary to the case of 2D semiconductors, transport at the charge neutrality point in the presence of puddles is still possible [41, 42]. The boundaries between these charge puddles are *pn* junctions which, for the case of graphene, have finite transparency. Transport close to the Dirac point has been successfully compared to percolating currents in networks of *pn* junctions [43], although the theoretical picture of transport at undoped graphene remains incomplete. Experiments of Refs. [41, 42], in agreement with previous numerical calculations [44], were able to give some values for the size and strength of the charge puddles. Consequently, the density fluctuations can be considered to have a characteristic length of up to 30 nm, with a measured strength of around 25–30 meV.

2.2 Superconductivity Basics I: Proximity Effect

Superconductivity is the mechanism by which many materials develop zero electrical resistance and perfect diamagnetism below a critical temperature and magnetic field value. The vanishing of electrical resistance was discovered by Kamerlingh Onnes [45] in 1911 while studying the properties of metals at extremely low temperatures. In 1933, Meissner and Ochsenfeld [46] measured the *expulsion* of magnetic fields by a material in the superconducting state. A phenomenological theory for this phenomenon, known as the Meissner effect, was developed by the London brothers in 1935 [47]. In 1954 Landau and Ginzburg published a phenomenological theory of superconductivity [48] in which they introduced the superconducting order parameter. A microscopic theory of superconductivity was formulated 46 years after its discovery by Bardeen, Cooper and Schrieffer (BCS theory [49]). In this theory, a phonon-mediated attractive interaction between electrons is the responsible for the transition into the superconducting state.

³ In the case of 2D semiconductors, the puddles are formed by either electrons or holes depending on the doping. In graphene at the Dirac point, the puddles are a mixture of electron and hole-doped inhomogeneities.

The main feature of superconductivity is the absence of resistance below a finite temperature T_C . Furthermore, the drop in the resistance is very sharp, implying a phase transition. According to the theory of conductivity [50], electrical resistance at finite temperature is dominated by the scattering of electrons by the vibrational excitations of the lattice (phonons). The phonons are continuously suppressed by lowering the temperature reaching a minimum at $T = 0$ where only the lattice defects and impurities contribute to the scattering of electrons. This result is independent of the temperature and insufficient to explain the appearance of superconductivity. The BCS microscopic theory of superconductivity demonstrates the formation of a new many-body ground state. In s-wave superconductors, Cooper pairs are formed by coupling two electron of opposite spin. The resulting pair has total spin 0 and can be considered a boson. Cooper pairs occupy the same many-body ground state. This is the BCS ground state which contains the sum of all Cooper pairs in the material. Since the Coulomb interaction causes a repulsive force between electrons, there has to be an attractive force between electron pairs in the conduction band. A weak, phonon-mediated, attractive interaction between electrons close to the Fermi surface is responsible for overcoming the Coulomb repulsion. Electrons in a metal create local distortions in the lattice, which act as an indirect attractive force upon other electrons. When this attraction overcomes the Coulomb repulsion, a Cooper pair is formed.

The ground state describes a collective excitation which includes all the individual Cooper pairs. The typical length scale of this collective mode ξ (the superconducting coherence length) is much greater than the mean distance between individual electrons in the metal and is a fundamental parameter that characterizes the superconductor. The collective mode provides a direct interpretation of the vanishing resistance of a superconductor. Since all individual Cooper pairs overlap at the ground state, the scattering of one of them requires an equivalent change of momentum in the rest. The amount of energy required is too large, and therefore the scattering of Cooper pairs is highly suppressed. The supercurrent given by the collective mode cannot be infinite since it is limited by the density of Cooper pairs. In the superconducting state, the attraction between electrons overcomes the Coulomb repulsion which makes the formation of Cooper pairs energetically favorable. The coupling between electrons opens a gap in the spectrum since it is impossible to have an individual excitation with energy below the one required to form a Cooper pair. The gap parameter Δ is another of the fundamental parameters in the characterization of a superconductor. The resulting ‘BCS density of states’ is

$$\frac{N_{BCS}(E)}{N(0)} = \begin{cases} \frac{|E-\mu|}{\sqrt{(E-\mu)^2 - \Delta^2}}, & |E - \mu| > \Delta \\ 0, & |E - \mu| < \Delta \end{cases} \quad (2.10)$$

where $N(0)$ represents the density of states on the normal state. In the inset of Fig. 2.2, we show the experimental results of Ref. [51] for the DOS of a bulk superconductor. It demonstrates that no quasi-particle is allowed below the superconducting gap

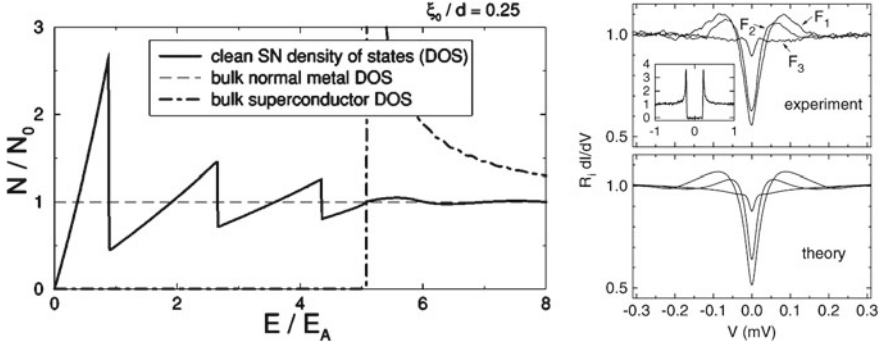


Fig. 2.2 Proximity effect in a normal-superconductor junction. *Left* Normalized DOS for the ballistic case. The bulk normal and superconductor cases are included. The bulk superconductor DOS is given by Eq. (2.10). Reprinted figure with permission from Pilgram et al. [55]. Copyright (2000) by the American Physical Society. *Right* Differential conductance in the tunnel regime for the diffusive case. The inset shows the bulk experimental results for the superconductor. Reprinted figure with permission from Guéron et al. [51]. Copyright (1996) by the American Physical Society

of width $2\Delta_{BCS}$. All the states are *pushed* to the edges of the gap, forming two characteristic peaks at $E - \mu = \pm\Delta$.

2.2.1 Proximity Effect on a Normal Metal-Superconductor Junction

A metal in electrical contact with a superconductor can develop superconducting features such as infinite conductance and perfect diamagnetism. We consider the superconductor as a reservoir where the electrons are condensed into Cooper pairs and the normal metal as a gas of free electrons. The proximity effect is the phenomenon in which the electrons in the normal metal acquire superconducting correlations through the diffusion at the contact between the normal metal and the superconductor. The behavior of the superconducting order parameter in the distances close to the interface is therefore crucial to study how the correlations leak into the normal region. Following the Ginzburg-Landau theory [48] a superconducting order parameter $\Delta(x)$, which only depends on the distance from the interface, contains all the information about the propagation of superconductivity into the normal region. This theory accounts for the macroscopic equilibrium properties close to the critical temperature, but it is not valid when $T \rightarrow 0$.

In the early 1960s, the simplest ballistic NS junction, an impurity-free normal metal on top of a superconductor, was solved exactly using the Bogoliubov-de Gennes equations (see a review in Ref. [52]). Subsequently, during the 1970s, the diffusive case was analyzed by Usadel [53]. That was the starting point for the development of what is known as the “nonequilibrium superconductivity theory” (a review can

be found in Ref. [54]). There, the order parameter $\Delta(x, E)$ contains both the spatial and the energy dependence of the density of states $N_{BCS}(x, E)$. In the absence of magnetic fields, the natural unit of length for the variation of $\Delta(x, E)$ is the superconducting coherence length ξ and the energy dependence is given by the density of states of the bulk superconductor $N_{BCS}(E)$. This theoretical prediction was confirmed by experiments on normal metal-superconductor nanoconstrictions carried on during the 1990s (a good example is Ref. [51]). Subsequently, experiments and theory reached a comparable level of maturity. Therefore, different scenarios have been understood at the microscopic level.

The ballistic case is characterized for having an electron mean free path l much greater than the superconducting coherence length ξ . The left panel of Fig. 2.2 shows the DOS of a junction formed by a finite normal metal on top of a superconductor calculated from the Bogoliubov-de Gennes equations (extracted from Ref. [55]). It also shows the constant density of states at the normal metal and a BCS-like density of states equivalent to Eq. (2.10). The DOS of the junction tends to the case of the isolated normal metal for an excitation energy greater than the gap value. Inside the gap, there is a finite DOS for energies greater than zero.

The diffusive regime is obtained when l is small compared with the superconducting coherence length. For this case we show in the right panel of Fig. 2.2 the experimental results of Ref. [51], in comparison with the theoretical predictions using Usadel equation. In this case, a semi-infinite normal metal has been coupled to the superconductor. The inset shows the experimental DOS for the bulk superconductor. In spite of having a well-defined BCS density of states, where the sharp edges at the gap can be observed, the DOS inside the normal region is smooth with a characteristic V-shaped dip at low voltages. For a diffusive NS junction, the number of states within the gap presents two maxima for energies close to the gap and is highly reduced at lower energies. The proximity effect is decreased with increasing distance from the interface.

2.3 Superconductivity Basics II: Andreev Reflection

2.3.1 The Concept of Andreev Reflection

At the interface between a normal metal and a superconductor, the superconducting pairing potential can convert an electron from the normal region into a hole, creating a Cooper pair in the superconductor. This process is known as Andreev reflection [56] and is responsible for transport in NS junctions. In a normal metal, the electron is a filled state with energy E above the Fermi energy E_F . If E is lower than the superconducting energy gap Δ , single-particle tunneling into the superconductor is forbidden since there are no available states. This quasi-particle may only enter the superconducting region if it forms a Cooper pair. In order to do that, it must couple with another electron from the normal region with opposite wave vector

and spin. The empty state below the Fermi energy left behind by this electron is the *reflected* hole. A total charge of $2e$ is transmitted from the normal region to the superconductor. Time-reversal symmetry yields that an incident hole from the normal region is Andreev-reflected as an electron at the interface.

This effect was first introduced by Andreev when studying the heat transport at NS interfaces [56]. Andreev reflection is the microscopic mechanism which explains how a dissipative current from the normal metal transforms into a supercurrent at the NS interface.

Most common metals have Fermi energies E_F that are much greater than the superconducting energy gap Δ .⁴ By neglecting the terms of the order Δ/E_F ,⁵ the incident electron and the reflected hole have the same wave vector which lies at the edge of the Fermi surface. While the velocity of a conduction band electron is parallel to its wave vector, the velocity of a conduction band hole is opposite to its wave vector and the hole is *retroreflected*. It is common to say that the hole traces back the path of the incident electron in the Andreev reflection.

2.3.2 Transport at a Normal Metal-Superconductor Interface

The Bogoliubov-de Gennes (BDG) equations describe the quasi-particle excitations in non-uniform superconductors. They are among the most useful techniques for describing phase-coherent transport in normal-superconductor (NS) hybrid structures. The quasi-particle excitations in a superconductor consist of a mixture of electron-like and hole-like states. The BDG equations are two coupled linear differential equations describing the amplitudes $u(x, E)$ and $v(x, E)$ of an excitation of energy E on the electron and hole states. They are expressed as,

$$\begin{pmatrix} H - E_F & \Delta(x) \\ \Delta^*(x) & E_F - THT^{-1} \end{pmatrix} \begin{pmatrix} u(x) \\ v(x) \end{pmatrix} = E \begin{pmatrix} u(x) \\ v(x) \end{pmatrix}, \quad (2.11)$$

where H is the single-particle Hamiltonian of the system (i.e. Schrödinger or Dirac-Weyl, depending on if we are describing traditional metals or graphene respectively), T is the time-reversal operator and $\Delta(x)$ is the pairing potential between electrons and holes.

A simple example system is a one-dimensional normal-superconductor junction with an insulating barrier at the interface (NIS system). By substituting H in (Eq. 2.11) by the Schrödinger Hamiltonian in one dimension and making $\Delta(x) = \Delta_0 \theta(x)$, with $\theta(x)$ being the Heaviside step function, we can describe an impurity-free one-dimensional junction with one normal region and one superconducting region. We can consider an incoming electron from the normal region into the super-

⁴ For example, Copper and Aluminum have Fermi energies of 7 and 11.7 eV, respectively [57]. On the other hand, the bulk superconducting gap of Aluminum is 0.18 meV [50].

⁵ This simplification is known as Andreev approximation.

conductor and allow it to be either transmitted as a Cooper pair or reflected as a hole. By matching wave functions at the interface we obtain that the Andreev reflection probability is⁶ $R_{eh} = |r_{eh}|^2 = |u_0/v_0|^2$. The probability of Andreev reflection is thus unity inside the superconducting gap and decays exponentially outside. This one-dimensional result is easily expanded for the 3D case, where electron normal reflection is included. In a famous article from 1982, Blonder, Tinkham and Klapwijk (BTK model [58]) used this formalism based on the BDG equations for the first time to describe superconducting microconstrictions. They solved the problem introduced here, using both plane waves to consider impurity-free systems and a Dirac delta-like potential at the point between the normal and the superconductor electrodes to include all the possible scattering processes at the interface. The intensity of the barrier is controlled by a parameter Z , which allows for the absence of barrier ($Z = 0$) as well

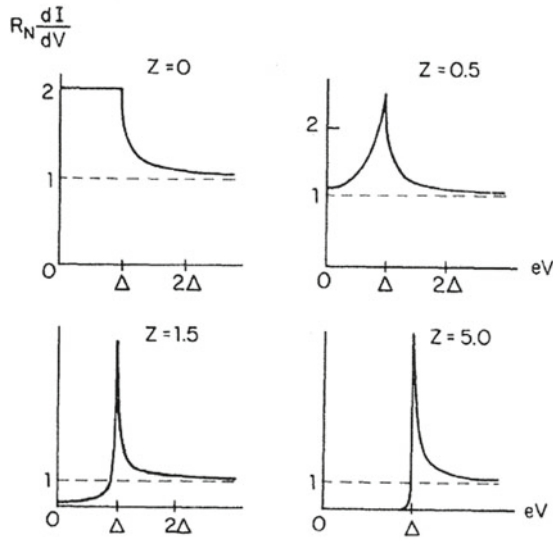


Fig. 2.3 Differential conductance as a function of the voltage at the metallic NIS junction for different values of the barrier intensity Z . Reprinted figure with permission from Blonder et al. [58]. Copyright (1982) by the American Physical Society

⁶ In the one-dimensional case, we consider plane wave solutions of Eq. (2.11) of the form $(u_0, v_0) \times e^{ik_S^e x}$, where $u_0^2(v_0^2) = \min[1, E/\Delta_0](1 \pm \sqrt{E^2 - \Delta_0^2}/E)/2$ are the BCS coherence factors and the wave vector has the form $k_S^{e,h}(E > 0) = \sqrt{2m(E_F^S \pm \sqrt{E^2 - \Delta_0^2})/\hbar^2}$. The wave vector for the normal region is obtained for $\Delta_0 \rightarrow 0$, limit in which (1, 0) and (0, 1) represent electron and hole quasi-particles, respectively. The matching of the wave functions reads

$$\begin{pmatrix} 1 \\ 0 \end{pmatrix} e^{ik_N^e x} + r_{eh} \begin{pmatrix} 0 \\ 1 \end{pmatrix} e^{ik_N^h x} = \begin{pmatrix} u_0 \\ v_0 \end{pmatrix} e^{ik_S^e x}.$$

The normalization is done over the incident flow and thus r_{eh} is the Andreev reflection amplitude.

as a strong barrier ($Z \gg 1$). By studying the probability of each microscopic process and its contribution to the current they obtained the conductance results shown in Fig. 2.3. The two limiting cases of zero barrier and strong barrier are very instructive. In the former, the probabilities of normal reflection and transmission of electrons into hole-like excitations are both zero. Thus, Andreev reflection for energies below the gap is perfect (i.e. occurs with unit probability as in the one-dimensional case) and transmission of electrons into the superconductor as electron-like excitations is $T_{ee} = 1 - R_{eh}$ (contributing to the conductance only for energies over the gap). This behavior is particular to metallic junctions. The Andreev reflection probability for strong barrier is strongly suppressed while normal reflection R_{ee} dominates inside the gap. This behavior is characteristic of classical tunnel junctions. In this way, the BTK model continuously connects this two limiting cases. The importance of this simple model was demonstrated by the experiments conducted by Blonder and Tinkham [59]. There is an excellent agreement between the theoretical predictions and the experimental $I - V$ curves for Cu-Nb point contacts.

2.3.3 Andreev Reflection in Graphene: Specular and Retro

When the Andreev reflection takes place, the transmitted Cooper pair must carry zero total momentum, so the electrons forming it belong to opposite corners of the Brillouin zone. Consequently, the Andreev reflection mixes graphene's valleys ($\pm \mathbf{K}$) [60]. The relativistic dispersion relation of graphene where the valence band and the conduction band touch at the Dirac points allows us to consider two limiting situations: $E_F < \Delta$ and $E_F > \Delta$, for an incident electron with $E > 0$. When $E < E_F$, which is the usual case of traditional NS junctions, the reflected hole remains in the conduction band (in graphene it still belongs to the other valley). Energy conservation requires that the reflected hole is located at $-E$, which is an empty state of the conduction band. The schematic of this *intraband* process is depicted in Fig. 2.4a. For the case with $E > E_F$, energy conservation demands that the reflected hole is in the valence band. The resulting *intraband* process is illustrated in Fig. 2.4b. Intraband processes do not exist in normal metals where the excitation gap is much greater than the superconducting gap [18].

An analysis of the dispersion relation of a graphene-superconductor junction supplies more information about these processes. Let the interface be at $x = 0$, with the graphene normal region at $x > 0$. The dispersion relation of an impurity-free graphene-based NS system in the mean-field approximation for superconductivity⁷ is

⁷ The mean-field approximation for superconductivity demands that the superconducting coherence length $\xi = \hbar v_F / \Delta$ is much greater than the Fermi wave length on the superconductor $\lambda_F^S = \hbar v_F / (E_F^S + U_0)$. There is no restriction over the relative magnitude of ξ and the Fermi wave length in the normal region. This approximation allows us to impose rigid boundary conditions on the pair potential $\Delta(x)$, with $\Delta(x) = \Delta$ in the superconducting region and $\Delta(x) = 0$ in the normal region.

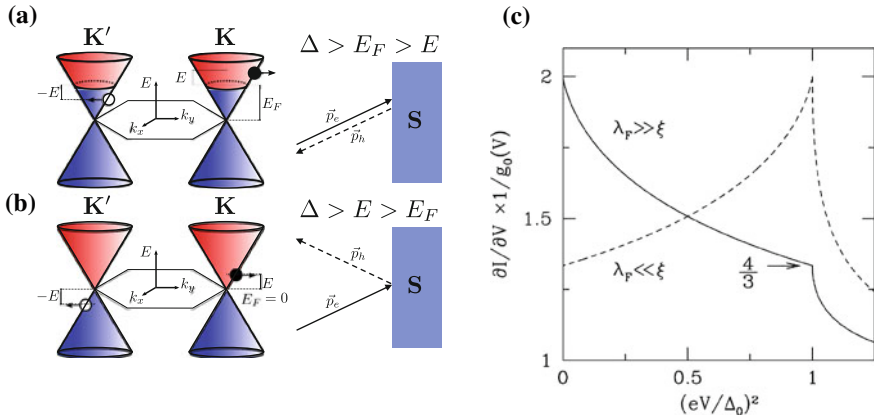


Fig. 2.4 Andreev reflection in graphene takes place when $E < \Delta$ with the incoming electron (full black circle) and the outgoing hole (empty circle) in different valleys. **a** Andreev retro-reflection occurs for $E_F > E$ and is dominant when $E_F \gg E, \Delta$. The electron and the hole are both in the conduction band. **b** Specular Andreev reflection occurs for $E > E_F$ and is dominant when $E_F \ll E, \Delta$. Contrary to the previous case, the reflected hole is in the valence band. **c** Differential conductance (normalized by the ballistic value g_0) of the interface between normal and superconducting graphene showing the regime in which retroreflection dominates ($\lambda_F = \hbar v_F / E_F \ll \xi = \hbar v_F / \Delta$) and that in which specular reflection dominates ($\lambda_F \gg \xi$). Reprinted figure with permission from Beenakker [60]. Copyright (2006) by the American Physical Society

$$E = \begin{cases} \sqrt{|\Delta|^2 + \left(E_F \pm \hbar v_F \sqrt{k_x^2 + k_y^2}\right)^2}, & x < 0 \\ |E_F \pm \hbar v_F \sqrt{k_x^2 + k_y^2}|, & x > 0 \end{cases} \quad (2.12)$$

The \pm sign identifies excitations from the conduction (+) and the valence (−) bands. The group velocity for a conduction band electron state with energy E is $V_e = k_e / |k_e|$. The group velocity for holes created at the same energy is $V_h = \mp k_h / |k_h|$, where the $- (+)$ sign corresponds to the conduction (valence) band. The different sign is obtained since the holes have the opposite group velocities of the electrons for a given momentum and there is a change of sign between the conduction and the valence bands. Thus, the group velocity and the momentum of a conduction band hole have opposite sign, while they have the same sign for a valence band hole. In the intraband reflection, the group velocity of the reflected hole has the opposite sign than the velocity of the incoming electron. Thus, Andreev reflection has a *retro*-reflection character as all components of the velocity change sign and the hole follows back the path of the incident electron (see right panel of Fig. 2.4a). On the contrary, in the interband reflection the group velocity of the reflected hole (in the valence band) is parallel to its momentum. A specular reflection takes place since the component of the momentum parallel to the interface (k_y) is conserved upon reflection. When $E_F = 0$, the reflected hole is always an empty state below the Fermi energy so, in undoped graphene, Andreev reflection is a specular (interband) process at all excitation energies (see Fig. 2.4b).

2.3.4 The BTK Model Applied to Graphene

In a seminal article by Beenakker in 2006 [60], the BTK model was applied to a graphene-based NS system. Substituting the Dirac-Weyl Hamiltonian of Eq. (2.6) into (2.11), we reach what are commonly known as the Dirac-Bogoliubov-de Gennes (DBdG) equations. The Fermi energy of a metal is much greater than other energy scales like the excitation energy and the superconducting gap. This means that both electron and hole states belong to the conduction band. Yet, the Fermi energy in graphene can be comparable or even smaller than the excitation energy and the gap. The conduction and the valence bands in graphene touch at the Dirac point and Andreev conversion of electrons into holes can occur in different bands. In Fig. 2.4c we show the plots of the conductance for a graphene-based NS junction, showing the two distinctive regimes of low-doping (which enhances interband Andreev reflection) and high-doping (which is mainly due to intra-band Andreev reflection and is equivalent to the metallic junction behavior with a small barrier). The study of the graphene NIS junction published in Ref. [61] highlighted another important difference with the metallic junctions: the conductance is an oscillatory function of the effective barrier strength. The amplitude of oscillations is maximum when the Fermi levels of the normal and the superconducting region are aligned and it can be zero for a large Fermi vector mismatch.⁸ In addition to that, a maximum value of the conductance can be reached at zero bias for a finite barrier, in stark contrast to the case of metallic junctions.

2.3.5 Nonlocal Transport and Crossed Andreev Reflection

Andreev reflection is intrinsically a nonlocal process. It takes place in a coherence volume of size ξ , the characteristic length associated with the superconducting gap Δ . Consequently, the incident electron and the reflected hole can be separated by hundreds of nanometers.

In an article published in 2000, Deutscher and Feinberg [63] considered a multi-terminal system formed by two point contacts coupled to a superconductor and separated by a distance L smaller than the superconducting coherence length (see the illustration in Fig. 2.5). When studying transport at subgap voltages and temperatures they realized that Cooper pairs made by electrons coming from each contact can be injected into the superconductor. This process is known as *crossed* Andreev reflection (CAR) (see Fig. 2.5a). It was further shown that another process involving the coherent tunneling of an electron from one normal electrode to the other is possible [64] (see Fig. 2.5b). This process is called electron elastic cotunneling (EC) and its contribution to the nonlocal conductance has the opposite sign than the one due to a CAR process. It can exactly cancel the CAR contribution in the tunnel regime. A *local* Andreev reflection can occur at each normal electrode at the same time, giving

⁸ For a detailed study of both the NS and the NIS cases see Ref. [62].

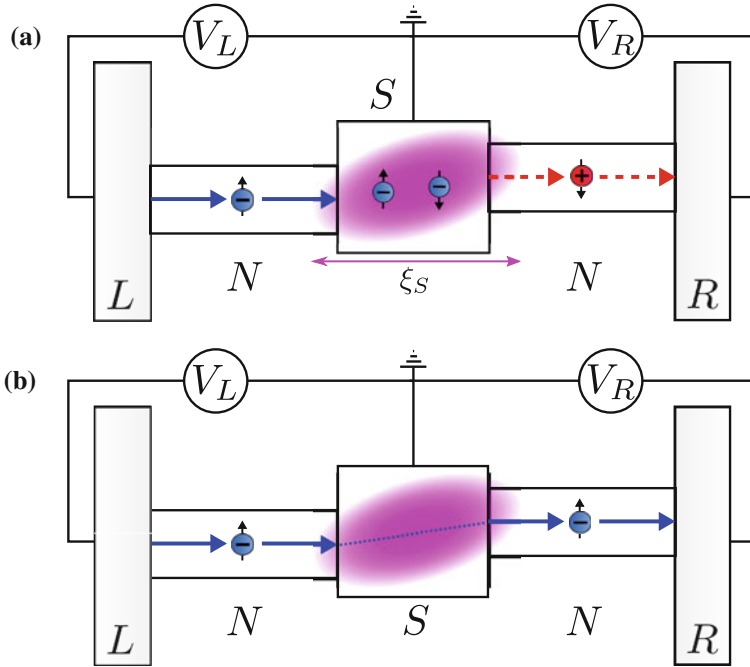


Fig. 2.5 Schematic of a three terminal device connected to a NSN system. The macroscopic electrodes L and R act as the source and drain, respectively. The superconductor S is grounded and a differential conductance can be measured between the electrodes. For performing a nonlocal transport measurement, the superconducting coherence length ξ_S must be comparable or bigger than the separation between the normal regions of the NSN junction. **a** Crossed Andreev reflection process: An electron from the source forms a Cooper pair inside the superconductor by coupling with an electron from the other normal region with opposite spin. The reflected hole is collected at the drain. **b** Electron elastic cotunneling process: An electron from the source performs a quantum coherent tunneling through the superconductor and into the drain

an extra contribution to the conductance of each electrode which is usually hard to distinguish from that arising from CAR processes.

Study of the nonlocal conductance can confirm the presence of CAR processes. The time-reversal of a CAR process is that in which each electron from a Cooper pair arriving from the superconductor coherently tunnels into a different normal electrode. An independent measurement of these processes is thus equivalent to measuring the splitting of a Cooper pair. As the total spin of the Cooper pair is zero the two electrons participating in this process are naturally spin entangled. Such splitting is therefore a source of entanglement and has many possible applications in quantum information theory.

The cancellation between the EC and the CAR contributions to the nonlocal conductance for thick tunnel barriers can be removed by introducing ferromagnetic leads [64, 65], increasing the barrier transparency [66–68] or taking into account

Coulomb interactions [69]. The importance of non-equilibrium effects at large bias voltages has also been analyzed [70].

A number of recent experiments have demonstrated these predictions. In 2004, Beckmann et al. [71] measured the nonlocal resistance of an Aluminum bar with two ferromagnetic wires forming point contacts to the Aluminum. When the Aluminum was in the superconducting state, they observed a nonlocal spin-dependent resistance. The spatial decay of this signal was controlled by the superconducting coherence length rather than the normal state spin-diffusion length. The energy dependence on the probability of EC and CAR was measured by Russo et al. [72]. They found that CAR dominated over EC at high energies, with the Thouless energy⁹ of the superconductor being the energy scale for the crossover. This indicates that the phase coherence of the processes plays a fundamental role in nonlocal transport. Further experiments corroborated this fact and confirmed the importance of the contact resistances and the excitation energy of the particles [73–75].

Another multi-terminal device was proposed by Recher et al. [76] in 2001. In this case, the superconductor was weakly coupled by tunnel barriers to two quantum dots (QDs). Each QD was treated as a one-level system and was also weakly coupled to a normal lead. If the QDs are in the Coulomb blockade regime, the probability for the state with two electrons on the same dot was suppressed. Electrons coming from the superconductor tunneled into separate dots and therefore into separate leads with higher probability. When the energy levels of the dots coincided, the splitting of the Cooper pairs from the superconductor was enhanced. The study of entanglement in similar systems was performed in Refs. [77] and [78]. Similar predictions were reached for other mesoscopic systems like Luttinger liquids [79].

References

1. P.R. Wallace, The band theory of graphite. *Phys. Rev.* **71**, 622–634 (1947) (Cited on Sects. 2.1 and 2.1.1)
2. J.C. Slonczewski, P.R. Weiss, Band structure of graphite. *Phys. Rev.* **109**, 272–279 (1958) (Cited on Sect. 2.1)
3. G.W. Semenoff, Condensed-matter simulation of a three-dimensional anomaly. *Phys. Rev. Lett.* **53**, 2449–2452 (1984) (Cited on Sect. 2.1)
4. S. Iijima, Helical microtubules of graphitic carbon. *Nature (London)* **354**, 56–58 (1991) (Cited on Sect. 2.1)
5. T. Ando, Theory of electronic states and transport in carbon nanotubes. *J. Phys. Soc. Jpn.* **74**, 777–817 (2005) (Cited on Sects. 2.1, 3.3, and D)
6. H. Boehm, R. Setton, E. Stumpp, Nomenclature and terminology of graphite-intercalation compounds (IUPAC recommendations 1994). *Pure Appl. Chem.* **66**, 1893–1901 (1994) (Cited on Sect. 2.1)

⁹ The Thouless energy is a characteristic energy scale of diffusive disordered conductors. It is defined by $E_T = \hbar D/L^2$, where D is the diffusion constant and L the size of the system, and thereby inversely proportional to the diffusion time $\tau_D = L^2/D$ through the system.

7. K. Novoselov, A. Geim, S. Morozov, D. Jiang, Y. Zhang, S. Dubonos, I. Grigorieva, A. Firsov, Electric field effect in atomically thin carbon films. *Science* **306**, 666 (2004) (Cited on Sect. 2.1 and 2.1.1)
8. K. Novoselov, D. Jiang, F. Schedin, T. Booth, V. Khotkevich, S. Morozov, A. Geim, Two-dimensional atomic crystals. *Proc. Natl. Acad. Sci. U. S. A.* **102**, 10451–10453 (2005) (Cited on Sects. 2.1 and 2.1.1)
9. K. Novoselov, A. Geim, S. Morozov, D. Jiang, M. Katsnelson, I. Grigorieva, S. Dubonos, A. Firsov, Two-dimensional gas of massless dirac fermions in graphene. *Nature* **438**, 197–200 (2005) (Cited on Sects. 2.1 and 2.1.1)
10. A.K. Geim, Graphene: status and prospects. *Science* **324**, 1530–1534 (2009) (Cited on Sect. 2.1)
11. H.B. Heersche, P. Jarillo-Herrero, J.B. Oostinga, L.M.K. Vandersypen, A.F. Morpurgo, Bipolar supercurrent in graphene. *Nature (London)* **446**, 56 (2007) (Cited on Sects. 2.1, 4.1, and 5.3.1)
12. A. Shailos, W. Nativel, A. Kasumov, C. Collet, M. Ferrier, S. Guéron, R. Deblock, H. Bouchiat, Proximity effect and multiple andreev reflections in few-layer graphene. *EPL (Europhys. Lett.)* **79**, 57008 (2007) (Cited on Sects. 2.1, 4.1, and 5.3.1)
13. F. Miao, S. Wijeratne, Y. Zhang, U.C. Coskun, W. Bao, C.N. Lau, Phase-coherent transport in graphene quantum billiards. *Science* **317**, 1530–1533 (2007) (Cited on Sects. 2.1, 4.1, and 5.3.1)
14. X. Du, I. Skachko, E.Y. Andrei, Josephson current and multiple Andreev reflections in graphene sns junctions. *Phys. Rev. B* **77**, 184507 (2008) (Cited on Sects. 2.1, 4.1, and 5.3.1)
15. A.H. Castro Neto, F. Guinea, N.M.R. Peres, K.S. Novoselov, A.K. Geim, The electronic properties of graphene. *Rev. Mod. Phys.* **81**, 109–162 (2009) (Cited on Sects. 2.1 and 4.4.3)
16. S. Das Sarma, S. Adam, E.H. Hwang, E. Rossi, Electronic transport in two-dimensional graphene. *Rev. Mod. Phys.* **83**, 407–470 (2011) (Cited on Sects. 2.1, 2.1.1, and B.2.3)
17. V. Gusynin, S. Sharapov, J. Carbotte, Ac conductivity of graphene: from tight-binding model to 2d+1-dimensional quantum electrodynamics. *Int. J. Mod. Phys. B* **21**, 4611–4658 (2007) (Cited on Sects. 2.1 and 3.3)
18. C.W.J. Beenakker, Colloquium: Andreev reflection and Klein tunneling in graphene. *Rev. Mod. Phys.* **80**, 1337–1354 (2008) (Cited on Sects. 2.1, 2.3.3, and B.1)
19. P. Allain, J. Fuchs, Klein tunneling in graphene: optics with massless electrons. *Eur. Phys. J. B: Condens. Matter Complex Syst.* **83**, 301–317 (2011) (Cited on Sect. 2.1)
20. F. Molitor, J. Güttinger, C. Stampfer, S. Dröschner, A. Jacobsen, T. Ihn, K. Ensslin, Electronic properties of graphene nanostructures. *J. Phys.: Condens. Matter* **23**, 243201 (2011) (Cited on Sects. 2.1 and 2.1.2)
21. A. Rozhkov, G. Giavaras, Y.P. Bliokh, V. Freilikher, F. Nori, Electronic properties of mesoscopic graphene structures: charge confinement and control of spin and charge transport. *Phys. Rep.* **503**, 77–114 (2011) (Cited on Sects. 2.1, 2.1.2, and 7)
22. P. Recher, B. Trauzettel, Quantum dots and spin qubits in graphene. *Nanotechnology* **21**, 302001 (2010) (Cited on Sects. 2.1 and 2.1.2)
23. E.R. Mucciolo, C.H. Lewenkopf, Disorder and electronic transport in graphene. *J. Phys.: Condens. Matter* **22**, 273201 (2010) (Cited on Sect. 2.1)
24. N.M.R. Peres, The transport properties of graphene. *J. Phys.: Condens. Matter* **21**, 323201 (2009) (Cited on Sect. 2.1)
25. T. Ando, T. Nakanishi, Impurity scattering in carbon nanotubes: absence of back scattering. *J. Phys. Soc. Jpn.* **67**, 1704–1713 (1998) (Cited on Sect. 2.1.2)
26. T. Ando, T. Nakanishi, R. Saito, Berry's phase and absence of back scattering in carbon nanotubes. *J. Phys. Soc. Jpn.* **67**, 2857–2862 (1998) (Cited on Sect. 2.1.2)
27. O. Klein, Die reflexion von elektronen an einem potentialsprung nach der relativistischen dynamik von dirac. *Zeitschrift für Physik A Hadrons Nuclei* **53**, 157–165 (1929) (Cited on Sect. 2.1.2)
28. M.I. Katsnelson, K.S. Novoselov, A.K. Geim, Chiral tunnelling and the Klein paradox in graphene. *Nat. Phys.* **2**, 620 (2006) (Cited on Sects. 2.1.2 and B.2.3)
29. B. Huard, J.A. Sulpizio, N. Stander, K. Todd, B. Yang, D. Goldhaber-Gordon, Transport measurements across a tunable potential barrier in graphene. *Phys. Rev. Lett.* **98**, 236803 (2007) (Cited on Sect. 2.1.2)

30. M. Lemme, T. Echtermeyer, M. Baus, H. Kurz, A graphene field-effect device. *IEEE Electron Device Lett.* **28**, 282–284 (2007) (Cited on Sect. 2.1.2)
31. B. Özyilmaz, P. Jarillo-Herrero, D. Efetov, D.A. Abanin, L.S. Levitov, P. Kim, Electronic transport and quantum hall effect in bipolar graphene p - n - p junctions. *Phys. Rev. Lett.* **99**, 166804 (2007) (Cited on Sects. 2.1.2 and 5.3.1)
32. J.R. Williams, L. DiCarlo, C.M. Marcus, Quantum hall effect in a gate-controlled p - n junction of graphene. *Science* **317**, 638–641 (2007) (Cited on Sect. 2.1.2)
33. E. Rossi, J.H. Bardarson, P.W. Brouwer, S. Das Sarma, Signatures of Klein tunneling in disordered graphene p - n - p junctions. *Phys. Rev. B* **81**, 121408 (2010) (Cited on Sect. 2.1.2)
34. V.V. Cheianov, V.I. Fal'ko, Selective transmission of dirac electrons and ballistic magnetoresistance of n - p junctions in graphene. *Phys. Rev. B* **74**, 041403 (2006) (Cited on Sect. 2.1.2)
35. A. De Martino, L. Dell'Anna, R. Egger, Magnetic confinement of massless dirac fermions in graphene. *Phys. Rev. Lett.* **98**, 066802 (2007) (Cited on Sect. 2.1.2)
36. M.I. Katsnelson, Zitterbewegung, chirality, and minimal conductivity in graphene. *Eur. Phys. J. B: Condens. Matter Complex Syst.* **51**, 157–160 (2006) (Cited on Sects. 2.1.2 and 4.2)
37. J. Tworzydło, B. Trauzettel, M. Titov, A. Rycerz, C.W.J. Beenakker, Sub-poissonian shot noise in graphene. *Phys. Rev. Lett.* **96**, 246802 (2006) (Cited on Sects. 2.1.2, 4.2, and B.2.3)
38. L. Brey, H.A. Fertig, Electronic states of graphene nanoribbons studied with the dirac equation. *Phys. Rev. B* **73**, 235411 (2006) (Cited on Sects. 2.1.2, 3.2.2, 3.2.3, 3.3.1, 3.3.2, 4.3.2, 4.3.4, and 4.3.1)
39. A.R. Akhmerov, C.W.J. Beenakker, Pseudodiffusive conduction at the dirac point of a normal-superconductor junction in graphene. *Phys. Rev. B* **75**, 045426 (2007) (Cited on Sects. 2.1.2, 4.1, and 4.3.1)
40. E. Prada, P. San-Jose, B. Wunsch, F. Guinea, Pseudodiffusive magnetotransport in graphene. *Phys. Rev. B* **75**, 113407 (2007) (Cited on Sects. 2.1.2 and 4.1)
41. J. Martin, N. Akerman, G. Ulbricht, T. Lohmann, J.H. Smet, K. Von Klitzing, A. Yacoby, Observation of electron-hole puddles in graphene using a scanning single-electron transistor. *Nat. Phys.* **4**, 144–148 (2008) (Cited on Sects. 2.1.2, 4.4.5, and 5.3.4)
42. Y. Zhang, V.W. Brar, C. Girit, A. Zettl, M.F. Crommie, Origin of spatial charge inhomogeneity in graphene. *Nat. Phys.* **5**, 722–726 (2009) (Cited on Sects. 2.1.2, 4.4.5, and 5.3.4)
43. V.V. Cheianov, V.I. Fal'ko, B.L. Altshuler, I.L. Aleiner, Random resistor network model of minimal conductivity in graphene. *Phys. Rev. Lett.* **99**, 176801 (2007) (Cited on Sect. 2.1.2)
44. E. Rossi, S. Das Sarma, Ground state of graphene in the presence of random charged impurities. *Phys. Rev. Lett.* **101**, 166803 (2008) (Cited on Sect. 2.1.2)
45. H. K. Onnes, *Comm. Phys. Lab. Univ. Leiden* 120b, 122b, 124c (1911) (Cited on Sect. 2.1.2)
46. W. Meissner, R. Ochsenfeld, Ein neuer effekt bei eintritt der supraleitfähigkeit. *Naturwissenschaften* **21**, 787–788 (1933) (Cited on Sect. 2.2)
47. F. London, H. London, The electromagnetic equations of the supraconductor. *Proc. R. Soc. Lond. Series A, Math. Phys. Sci.* **149**, 71–88 (1935) (Cited on Sect. 2.2)
48. V.L. Ginzburg, L.D. Landau *Zh. Eksp. Teor. Fiz.* **20**, (1950) (Cited on Sects. 2.2 and 2.2.1)
49. J. Bardeen, L.N. Cooper, J.R. Schrieffer, Theory of superconductivity. *Phys. Rev.* **108**, 1175–1204 (1957) (Cited on Sect. 2.2)
50. C. Kittel, *Introduction to Solid State Physics* (Wiley, New York, 1953) (Cited on Sects. 2.2 and 4)
51. S. Guéron, H. Pothier, N.O. Birge, D. Esteve, M.H. Devoret, Superconducting proximity effect probed on a mesoscopic length scale. *Phys. Rev. Lett.* **77**, 3025–3028 (1996) (Cited on Sects. 2.2 and 2.2.1)
52. P. de Gennes, *Superconductivity of Metals and Alloys* (Benjamin, New York, 1966) (Cited on Sect. 2.2.1)
53. K.D. Usadel, Generalized diffusion equation for superconducting alloys. *Phys. Rev. Lett.* **25**, 507–509 (1970) (Cited on Sect. 2.2.1)
54. J. Rammer, H. Smith, Quantum field-theoretical methods in transport theory of metals. *Rev. Mod. Phys.* **58**, 323–359 (1986) (Cited on Sects. 2.2.1 and A.2)

55. S. Pilgram, W. Belzig, C. Bruder, Excitation spectrum of mesoscopic proximity structures. *Phys. Rev. B* **62**, 12462–12467 (2000) (Cited on Sect. 2.2.1)
56. A. Andreev, *Zh. Eksp. Teor. Fiz.* **46** (1968) [*Sov. Phys. JETP* **19**, 1228 (1964)] (Cited on Sect. 2.3.1)
57. N. Ashcroft, N. Mermin, *Solid State Physics* (Harcourt College Publishers, Orlando, 1976) (Cited on Sect. 4)
58. G.E. Blonder, M. Tinkham, T.M. Klapwijk, Transition from metallic to tunneling regimes in superconducting microconstrictions: excess current, charge imbalance, and supercurrent conversion. *Phys. Rev. B* **25**, 4515–4532 (1982) (Cited on Sects. 2.3.2, 4.2.2, and 4.4.1)
59. G.E. Blonder, M. Tinkham, Metallic to tunneling transition in cu-nb point contacts. *Phys. Rev. B* **27**, 112–118 (1983) (Cited on Sect. 2.3.2)
60. C.W.J. Beenakker, Specular Andreev reflection in graphene. *Phys. Rev. Lett.* **97**, 067007 (2006) (Cited on Sects. 2.3.3, 2.3.4, 4.1, 4.2, 4.2.2, 4.4.1, 4.5, and 5.2)
61. S. Bhattacharjee, K. Sengupta, Tunneling conductance of graphene nis junctions. *Phys. Rev. Lett.* **97**, 217001 (2006) (Cited on Sects. 2.3.4, 4.1, 4.4.2, 5.3.3, and C)
62. J. Linder, A. Sudbø, Tunneling conductance in *s*- and *d*-wave superconductor-graphene junctions: extended Blonder-Tinkham-Klapwijk formalism. *Phys. Rev. B* **77**, 064507 (2008) (Cited on Sects. 8, 4.1, 5.3.3, and C)
63. G. Deutscher, D. Feinberg, Coupling superconducting-ferromagnetic point contacts by Andreev reflections. *Appl. Phys. Lett.* **76**, 487–489 (2000) (Cited on Sects. 2.3.5, 5.3.1, and 6.1)
64. G. Falci, D. Feinberg, F.W.J. Hekking, Correlated tunneling into a superconductor in a multi-probe hybrid structure. *EPL (Europhys. Lett.)* **54**, 255 (2001) (Cited on Sects. 2.3.5, 6.1, and 6.3.2)
65. R. Mélin, D. Feinberg, Sign of the crossed conductances at a ferromagnet/superconductor/ferromagnet double interface. *Phys. Rev. B* **70**, 174509 (2004) (Cited on Sects. 2.3.5, 6.1, and 6.3.2)
66. J.P. Morten, A. Brataas, W. Belzig, Circuit theory of crossed Andreev reflection. *Phys. Rev. B* **74**, 214510 (2006) (Cited on Sects. 2.3.5 and 6.1)
67. M.S. Kalenkov, A.D. Zaikin, Nonlocal Andreev reflection at high transmissions. *Phys. Rev. B* **75**, 172503 (2007) (Cited on Sects. 2.3.5 and 6.1)
68. R. Mélin, F.S. Bergeret, A.L. Yeyati, Self-consistent microscopic calculations for nonlocal transport through nanoscale superconductors. *Phys. Rev. B* **79**, 104518 (2009) (Cited on Sects. 2.3.5 and 6.1)
69. A.L. Yeyati, F.S. Bergeret, A. Martín-Rodero, T.M. Klapwijk, Entangled Andreev pairs and collective excitations in nanoscale superconductors. *Nat. Phys.* **3**, 455 (2007) (Cited on Sects. 2.3.5 and 6.1)
70. F.S. Bergeret, A. Levy Yeyati, Nonlocal transport through multiterminal diffusive superconducting nanostructures. *Phys. Rev. B* **80**, 174508 (2009) (Cited on Sects. 2.3.5 and 6.1)
71. D. Beckmann, H.B. Weber, H.V. Löhneysen, Evidence for crossed Andreev reflection in superconductor-ferromagnet hybrid structures. *Phys. Rev. Lett.* **93**, 197003 (2004) (Cited on Sects. 2.3.5 and 6.1)
72. S. Russo, M. Kroug, T.M. Klapwijk, A.F. Morpurgo, Experimental observation of bias-dependent nonlocal Andreev reflection. *Phys. Rev. Lett.* **95**, 027002 (2005) (Cited on Sects. 2.3.5 and 6.1)
73. P. Cadden-Zimansky, V. Chandrasekhar, Nonlocal correlations in normal-metal superconducting systems. *Phys. Rev. Lett.* **97**, 237003 (2006) (Cited on Sects. 2.3.5 and 6.1)
74. A. Kleine, A. Baumgartner, J. Trbovic, C. Schoenenberger, Contact resistance dependence of crossed Andreev reflection. *EPL (Europhys. Lett.)* **87**, 27011 (2009) (Cited on Sects. 2.3.5 and 6.1)
75. J. Wei, V. Chandrasekhar, Positive noise cross-correlation in hybrid superconducting and normal-metal three-terminal devices. *Nat. Phys.* **6**, 494–498 (2010) (Cited on Sects. 2.3.5 and 6.1)
76. P. Recher, E.V. Sukhorukov, D. Loss, Andreev tunneling, coulomb blockade, and resonant transport of nonlocal spin-entangled electrons. *Phys. Rev. B* **63**, 165314 (2001) (Cited on Sects. 2.3.5, 6.1, and 6.2)

- 77. N.M. Chtchelkatchev, G. Blatter, G.B. Lesovik, T. Martin, Bell inequalities and entanglement in solid-state devices. *Phys. Rev. B* **66**, 161320 (2002) (Cited on Sects. 2.3.5 and 6.1)
- 78. P. Samuelsson, E.V. Sukhorukov, M. Büttiker, Orbital entanglement and violation of bell inequalities in mesoscopic conductors. *Phys. Rev. Lett.* **91**, 157002 (2003) (Cited on Sects. 2.3.5 and 6.1)
- 79. C. Bena, S. Vishveshwara, L. Balents, M.P.A. Fisher, Quantum entanglement in carbon nanotubes, *Phys. Rev. Lett.* **89** 037901 (2002) (Cited on Sects. 2.3.5 and 6.1)

Superconductivity in Graphene and Carbon Nanotubes

Proximity effect and nonlocal transport

Burset Atienza, P.

2014, XIX, 157 p. 43 illus., 7 illus. in color., Hardcover

ISBN: 978-3-319-01109-7